Corrosion Science 53 (2011) 3058–3067

Contents lists available at ScienceDirect

Corrosion Science

journal homepage: www.elsevier.com/locate/corsci

Theoretical and electrochemical assessment of inhibitive behavior of some thiophenol derivatives on mild steel in HCl

A. Kosari [a], M. Momeni [a], R. Parvizi [a], M. Zakeri [a], M.H. Moayed [a,*], A. Davoodi [b], H. Eshghi [c]

[a] Materials and Metallurgical Engineering Department, Faculty of Engineering, Ferdowsi University of Mashhad, Mashhad 91775-1111, Iran
[b] Materials Engineering Department, Sabzevar Tarbiat Moallem University, Sabzevar 391, Iran
[c] Chemistry Department, Faculty of Science, Ferdowsi University of Mashhad, Mashhad 91775-1111, Iran

ARTICLE INFO

Article history:
Received 8 November 2010
Accepted 5 May 2011
Available online 10 May 2011

Keywords:
A. Mild steel
B. EIS
B. Polarization
C. Acid inhibition

ABSTRACT

Inhibitive performance of some synthesized thiophenol derivatives on corrosion behavior of mild steel in 0.1 M HCl solution was investigated by means of electrochemical techniques, quantum chemical and optical microscopy. The increase in concentration and immersion time shows a positive effect on inhibition efficiency while temperature has a negative effect. Inhibitor molecules directly adsorb at surface on the basis of donor–acceptor interactions between the π-electrons of benzene, sulfur and nitrogen atoms and the vacant *d*-orbitals of iron atoms. According to the thermodynamic parameters, present inhibitors adsorb physically. Optical microscopy examinations demonstrate a decrease in corrosion attacks in presence of inhibitors.

1. Introduction

Inhibitor is a keyword in the case of corrosion prevention by changing the chemistry of corrosive media. Many industrial divisions such as acid cleaning bath, water cooling system, various refinery units, pipelines, chemical operations, steam generators, ballast tanks, oil and gas production units are involved with inhibitors due to high corrosion rates in these parts. Regarding their vast applications, one could obviously obtain special importance of inhibitors in various industries. Hence, many researchers are trying to introduce new organic compounds which are more efficient, cost effective with easy access [1–7].

It is believed that inhibitors efficiency basically refers to their molecular structure [2,4,8–14]. Existence of unique atoms like N, O and S in heterocyclic compounds has been widely reported as an effective parameter in improvement of inhibitors efficiency in acidic media [15–19]. The structure and the lone electron pairs in the heteroatoms are important characteristics that determine the adsorption mechanism of these molecules on a metallic surface [20]. Nevertheless, other parameters such as environmental characteristics, nature of the metal and other experimental conditions can play important roles in their efficiency [8,20–23]. Generally, organic inhibitor molecules might physically or chemically adsorb on a corroding metal. In any case, adsorption is general over the metal surface and the resultant adsorbed layer functions as a barrier which isolates the exposed metal from further deterioration.

In addition to traditional techniques such as electrochemical and gravimetric measurements, recently, quantum chemical method has been employed in inhibitors study. Invaluable quantum chemical parameters such as higher occupied molecular orbital (HOMO), lower unoccupied molecular orbital (LUMO) and dipole momentum (μ) obtained by this method, help to understand the adsorption properties by considering the structure of every individual molecule.

The choice of inhibitors (Fig. 1) in this study is based on their different molecular structures while their building atoms are similar. Consequently, it could be claimed that the variation in inhibitive properties refers to the difference in their molecular structure. Quantum chemical and several electrochemical methods have been employed to assess the inhibitive behavior of these thiophenol derivatives on mild steel samples in HCl solution.

2. Experimental methods

2.1. Materials

All the experiments were performed on mild steel with the chemical composition (in wt.%) presented as follows: 0.16% C, 0.1% Si, 0.4% Mn, 0.02% S, 0.13% P and Fe balance. The working electrode, with 2.5 cm^2 exposed area, was made by cold mounting of a rod mild steel sample with a self-cure epoxy resin. Before each test, specimens were mechanically ground down to 1000 grit abrasive SiC paper, then washed in deionized water and dried with hot air. The electrolyte solution, 0.1 M HCl, was prepared by Merck

* Corresponding author. Tel.: +98 511 876 3305; fax: +98 511 876 3302.
E-mail address: mhmoayed@um.ac.ir (M.H. Moayed).

0010-938X/$ - see front matter © 2011 Elsevier Ltd. All rights reserved.
doi:10.1016/j.corsci.2011.05.009

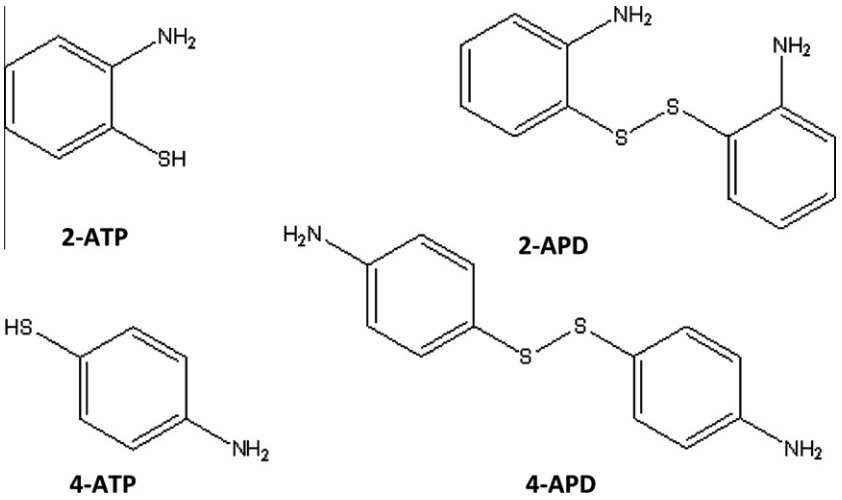

Fig. 1. Molecular structures of inhibitors.

reagent and deionized water. The tests were performed at various temperatures (with ±1 °C accuracy) controlled by using a water bath.

2.2. Inhibitors preparation and characterization

Inhibitors 2-aminophenyl disulfide (2-APD) and 4-aminophenyl disulfide (4-APD) were synthesized according to the previously reported procedure [24]. A mixture of 2-aminothiophenol (2-ATP) or 4-aminothiophenol (4-ATP) (10 mmol), DMSO (30 mmol) and $Fe(HSO_4)_3$ (0.35 g, 1 mmol) in ethanol (50 ml) was stirred at room temperature for 1 h. After completion of the synthesis procedure, the reacted mixture was filtered and the organic solvent was removed. The residue was then dissolved in CH_2Cl_2 (5 ml), washed with water (2× 10 ml), and dried with anhydrous Na_2SO_4. After solvent evaporation, the corresponding 2-APD and 4-APD were obtained in 95% and 85% yields. Characterizations of these two synthesized compounds are as follows [23]:

2.2.1. 2-Aminophenyl disulfide (2-APD)

Melting point 88–91 °C, ^{1}H NMR (100 MHz, DMSO-d^6): δ = 7.1–7.3 (complex, 4H), 6.5–6.8 (complex, 4H), 3.8–4.2 (brs, 4H). IR (KBr, cm^{-1}): 3350, 3280, 3100, 1620, 1490, 1425, 1285, 1195, 1075, 830, 690, 620, 530.

2.2.2. 4-Aminophenyl disulfide (4-APD)

Melting point 76–79 °C, ^{1}H NMR (100 MHz, $CDCl_3$): δ = 7.3 (d, J = 8.7 Hz, 4H), 6.6 (d, J = 8.7 Hz, 4H), 3.7 (brs, 4H). IR (KBr, cm^{-1}): 3400, 3300, 3100, 1620, 1480, 1430, 1280, 1195, 1080, 820, 690, 620, 520.

2.3. Electrochemical measurements

The electrochemical tests have been performed using Gill AC laboratory potentiostat (ACM instrument). Electrochemical measurements have been carried out in a conventional three-electrode cell configuration in which mild steel was used as working electrode, saturated calomel electrode (SCE) and a platinum wire as reference and auxiliary electrodes, respectively. Before each test, the working electrode was immersed for 45 min in solution to obtain a steady state open circuit potential (OCP). Linear polarization resistance (LPR) test have been accomplished at constant sweep rate (10 mV/min) with scanning range from −15 to +15 mV around OCP. The LPR values have been measured by calculating the slope of the linear part of current–potential plot. Potentiodynamic polarization curves have been recorded at constant sweep rate of 1 mV/s in which the scanning range was altered from −250 to +250 mV around the OCP. Electrochemical impedance spectroscopy (EIS) measurements have been carried out in frequency range of 100 kHz to 0.01 Hz with amplitude of 15 mV peak-to-peak using AC signals at OCP.

2.4. Corrosion attack morphology investigation

In order to investigate the effect of inhibitors on corrosion morphology, optical microscope has been employed. The specimen surface was mechanically polished down to 0.05 μm alumina slurry. Then, they were immersed in 0.1 M HCl in absence and presence of 200 ppm (mg/l) of various inhibitors for 90 min at ambient temperature. After eliciting of each specimen from solution, it was washed and cleaned by ethanol and immediately dried with warm air.

2.5. Quantum chemical study

The molecular structures of the 2-ATP, 4-ATP, 2-APD and 4-APD have been geometrically optimized by DFT method using B3LYP level and 3–21G** basis set with Gaussian 98. Quantum chemical parameters such as the highest occupied molecular orbital (HOMO) and the lowest unoccupied molecular orbital (LUMO) have been calculated.

3. Results and discussion

3.1. Effect of inhibitor concentration

3.1.1. Potentiodynamic polarization

Fig. 2 shows polarization curves for mild steel in 0.1 M HCl at 25 °C after 1 h immersion at various concentrations of 2-ATP, 4-ATP, 2-APD and 4-APD. Electrochemical parameters which could be extracted from polarization curves such as corrosion potential (E_{corr}), corrosion current density (i_{corr}), anodic and cathodic Tafel slopes (β_a and β_c) are measured by Tafel extrapolation and presented in Table 1. Also, considering the corrosion current densities in absence (i^0_{corr}) and presence of inhibitor (i_{corr}), values of surface coverage (θ) and inhibitor efficiency ($\%\eta$) is calculated by means of the following equations:

$$\theta = \frac{i^0_{corr} - i_{corr}}{i^0_{corr}} \quad (1)$$

$$\%\eta = \theta \times 100 \quad (2)$$

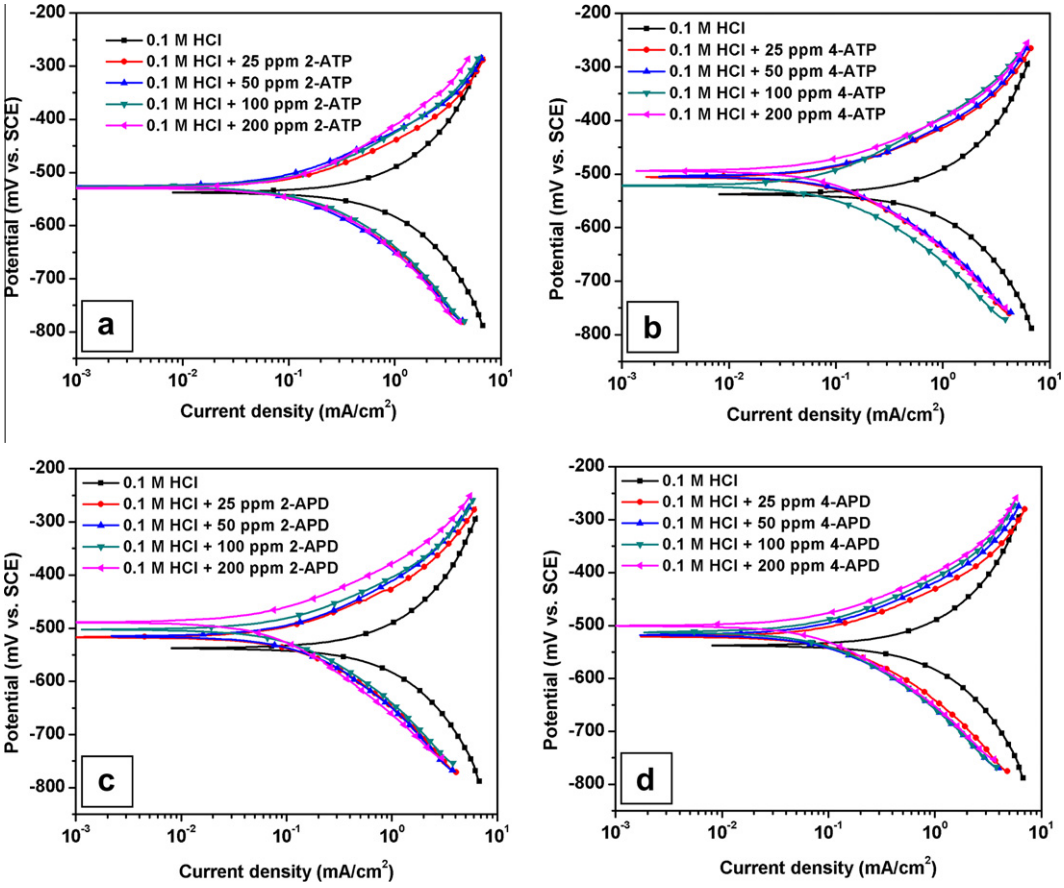

Fig. 2. Potentiodynamic polarization of (a) 2-ATP, (b) 4-ATP, (c) 2-APD and (d) 4-APD in various concentrations at 25 °C.

Table 1
Electrochemical parameters obtained from the polarization curves of (a) 2-ATP, (b) 4-ATP, (c) 2-APD and (d) 4-APD at 25 °C.

Inhibitor	Concentration (ppm)	E_{corr} (mV vs. SCE)	i_{corr} (mA/cm^2)	β_a (mV/decade)	$-\beta_c$ (mV/decade)	θ	$\%\eta$
	Blank	−536	1.06	279	267	–	–
2-ATP	25	−507	0.20	135	177	0.81	81
	50	−504	0.19	136	164	0.82	82
	100	−501	0.17	135	164	0.84	84
	200	−494	0.14	121	160	0.86	86
4-ATP	25	−532	0.22	132	172	0.79	79
	50	−526	0.21	131	181	0.80	80
	100	−527	0.19	125	170	0.82	82
	200	−528	0.19	143	185	0.82	82
2-APD	25	−520	0.26	140	216	0.75	75
	50	−508	0.18	132	165	0.83	83
	100	−501	0.16	130	172	0.85	85
	200	−479	0.07	109	140	0.93	93
4-APD	25	−527	0.26	141	179	0.76	76
	50	−517	0.15	120	163	0.86	86
	100	−513	0.14	124	160	0.87	87
	200	−499	0.13	120	154	0.88	88

It should be noticed that in some curves, anodic branch does not show a complete linear Tafel behavior, especially anodic branch of the curves obtained from bulk solution. But, almost all the cathodic branches show linear behavior at potentials lower than 100 mV below the corrosion potential. To measure the anodic Tafel slope of those curves, e.g. bulk solution anodic Tafel slope, a method which has been previously reported by McCafferty [25] was employed (Fig. 3).

In this method, if both anodic and cathodic Tafel lines show linear behavior, by extrapolating of lines to corrosion potential and calculating their slope, cathodic and anodic Tafel slopes can be calculated and also corrosion current density is measured from the cross-point of the two lines.

In addition, it is possible to calculate the corrosion potential, corrosion current density and anodic and cathodic Tafel slopes if there is at least one branch under activation control. For this purpose, the branch that shows linear behavior is considered. In this study, cathodic branch shows linear behavior at potentials lower than 100 mV below corrosion potential. This linear part of cathodic curve is extended to positive potentials (see Fig. 3) and then,

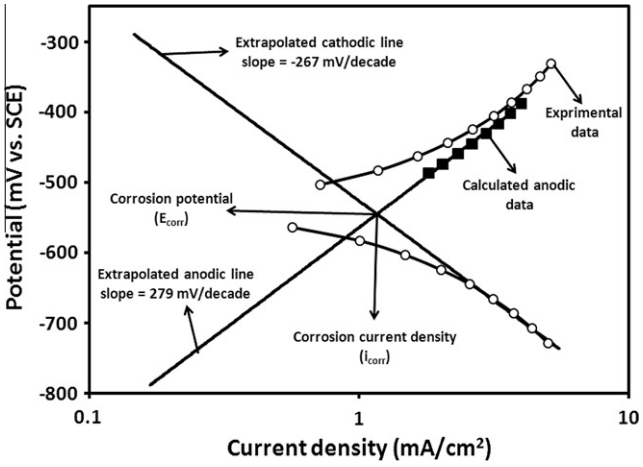

Fig. 3. Extrapolation method applied for measuring Tafel slopes, corrosion potential and corrosion current density.

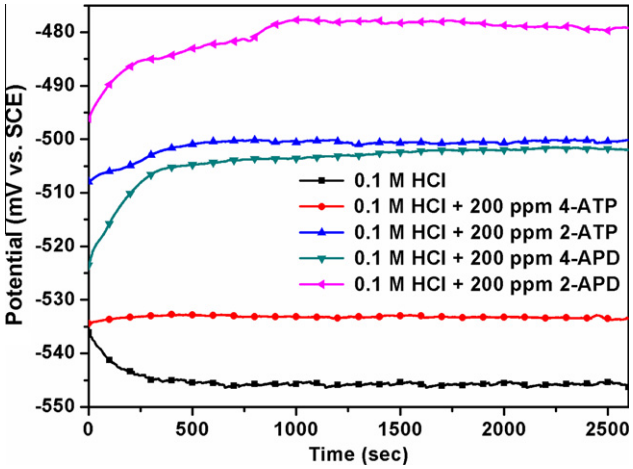

Fig. 4. Effect of present inhibitors at 200 ppm concentration on corrosion potential.

considering negative and positive signs for cathodic and anodic currents, respectively, the anodic current density (i_a) is calculated from the net current density (i_{net}) and cathodic current density (i_c) at anodic potentials by the following equation:

$$i_a = i_{net} - i_c \tag{3}$$

Afterward, by linear extrapolating the calculated anodic data to more negative potentials with respect to corrosion potential, the anodic Tafel slope can be calculated. In addition, the current density and potential at the intercept of two extrapolated lines shows corrosion current density and corrosion potential, respectively.

Assessment of Table 1 data shows a considerable decrease in corrosion rate in presence of inhibitors in comparison with blank solution. Considering the optimum concentration, 200 ppm (the highest obtained efficiency among the investigated concentrations for all inhibitors), they can be listed from efficiency in order of 2-APD > 4-APD > 2-ATP > 4-ATP. Fig. 2 reveals that the net cathodic current density in presence of all inhibitors is nearly independent of inhibitor concentration. However, it seems that the net anodic current density decreases by increasing the inhibitor concentration especially in the case of 2-APD. An increase in inhibitor concentration tends to block more anodic sites which are suitable for metal dissolution. Adsorption of organic inhibitor molecules onto a metal surface and therefore retarding of metal dissolution and as a consequence hydrogen evolution by blocking available sites is widely accepted by other researchers [5,9–10,13,18,26]. Although totally blocking of active sites have been proposed by several authors, but, the presence of defects in an organic layer created by adsorption cannot be ruled out. Therefore, hydrogen evolution and metal dissolution may occur from these areas with no inhibitor coverage $(1-\theta)$ [26]. A linear relationship between applied overpotential and net cathodic current density reveals that the hydrogen evolution is under activation-control and the reduction mechanism is not changed at the presence of inhibitors [13]. The variation of β_c values with altering in type and concentration of inhibitors indicates the influence of compounds on the kinetics of hydrogen evolution. Also, the shift in the anodic Tafel slope (β_a) may be due to the chloride ions/or inhibitor modules adsorbed onto the steel surface [27]. The anodic curves show that the tested compounds have lower inhibitive effect at +200 mV with respect to E_{corr}. This phenomenon can be related to the significant metal dissolution at this potential leading to desorption of the inhibiting layer [28]. Although present inhibitors decrease both the anodic and cathodic current densities, they are classified as anodic inhibitors due to shifting the rest potential toward more positive values (Fig. 4).

3.1.2. Electrochemical impedance spectroscopy

Electrochemical impedance spectroscopy (EIS) has been employed in order to investigate the surface layer created by inhibitors. The effect of inhibitor concentration on the impedance behavior of mild steel in 0.1 M HCl at 25 °C has been exhibited in Fig. 5. Nyquist plots for mild steel at various concentrations of all inhibitors are nearly similar and contain a depressed semicircle at higher frequencies that is related to the charge transfer process. An increase in semi-circle diameter is indicating an increase in corrosion resistance of mild steel in presence of inhibitors. In addition, in the case of 2-APD and 4-APD an inductive loop is observed at low frequency part. Existence of this loop could be derived from adsorbed intermediate products such as $(FeCl^-)_{ads}$ in absence and/or $(FeCl^-\ Inh^+)_{ads}$ presence of inhibitors [29]. Even though, this loop at lower frequencies can be attributed to the local desorption of inhibitor from surface.

The extracted impedance parameters analyzed by EIS analyzer software from EIS plots, are listed in Table 2. Inhibitor efficiency can also be estimated by charge transfer resistance according to the following formula [8–9]:

$$\%\eta = \frac{R - R^0}{R} \times 100 \tag{4}$$

where R^0 and R are charge transfer resistance of mild steel in absence and presence of the inhibitor, respectively. Calculated efficiency by charge transfer resistance is in close correlation with those obtained from polarization results. Furthermore, values of CPE capacitance were calculated by the following equation [30]:

$$C_{dl} = P^{1/n} R_{ct}^{1-n/n} \tag{5}$$

In above expressions, P, ω and n are the magnitude of CPE, the angular frequency and deviation parameter, respectively. Generally, the values of double-layer capacitance (C_{dl}) decrease by adding inhibitors, but no certain uniformity is seen in the increase or decrease of C_{dl} capacitance by increasing the inhibitors concentration. According to Helmholtz model, double layer capacitance is inversely proportional to the surface film thickness [31].

$$C_{dl} = \frac{\varepsilon_0 \varepsilon}{d} S \tag{6}$$

where d is the film thickness, S is the electrode surface, ε_0 is the permittivity of air and ε is the local dielectric constant. The decrease in C_{dl} is probably due to a decrease in local dielectric constant and/or an increase in thickness of the protective layer formed at electrode surface [32]. Although, the decrease in surface area (which acts as a site for charging) may also be the another reason for C_{dl} decreasing

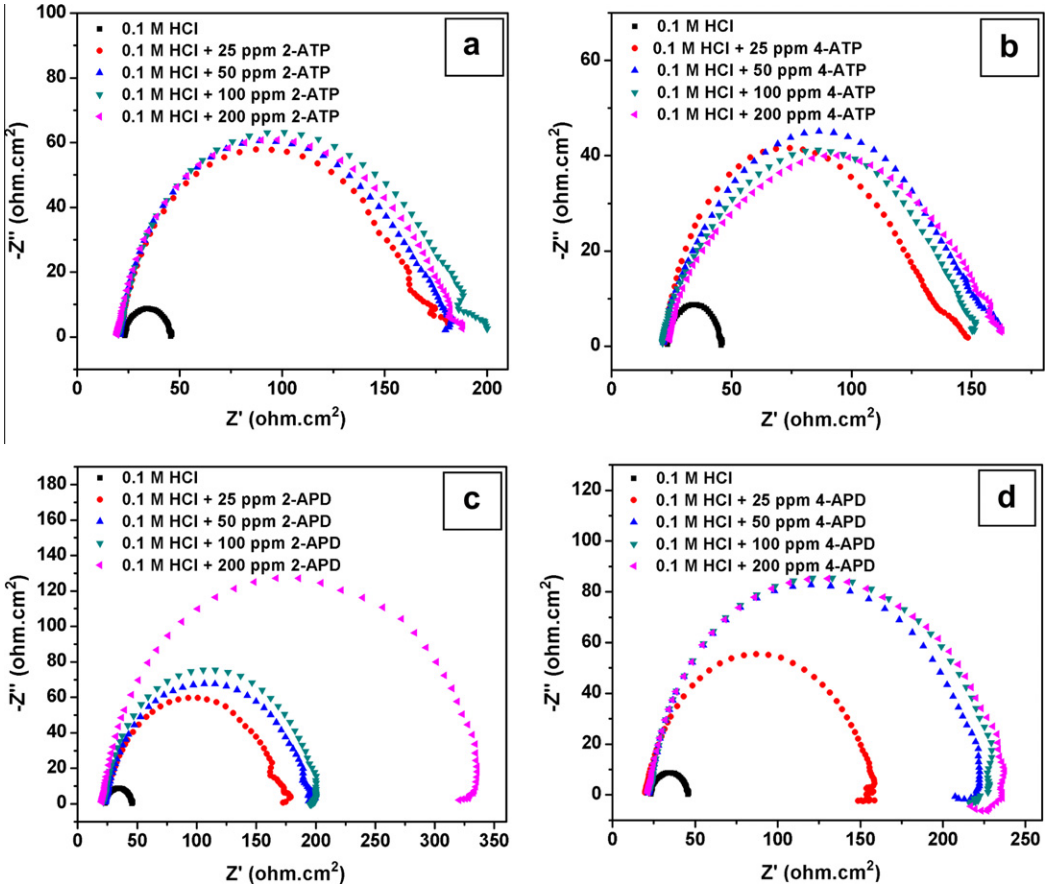

Fig. 5. Nyquist plot of (a) 2-ATP, (b) 4-ATP, (c) 2-APD and (d) 4-APD in different concentrations at 25 °C.

Table 2
Impedance parameters data and LPR results for mild steel in 0.1 M HCl without and with different concentration of thiophenol derivatives at 25 °C.

Inhibitor	Concentration (ppm)	EIS							LPR		
		R_s (Ω cm^2)	R_{ct} (Ω cm^2)	CPE_{dl}		C_{dl} (μF/cm^2)	θ	%η	LPR (Ω cm^2)	θ	%η
				P (μF/cm^2)	n						
	Blank	23	23	450	0.83	176.7	–	–	46	–	–
2-ATP	25	21	148	138	0.86	73.2	0.84	84	186	0.75	75
	50	21	156	139	0.86	74.5	0.85	85	182	0.75	75
	100	20	166	139	0.86	75.3	0.86	86	202	0.77	77
	200	20	161	140	0.86	75.5	0.86	86	204	0.77	77
4-ATP	25	20	115	200	0.83	92.4	0.80	80	144	0.68	68
	50	23	132	258	0.78	99.3	0.82	82	156	0.70	70
	100	20	133	490	0.71	160.6	0.83	83	148	0.70	70
	200	20	141	520	0.67	143.6	0.84	84	160	0.71	71
2-APD	25	23	151	138	0.86	73.5	0.85	85	161	0.71	71
	50	22	182	108	0.89	66.5	0.87	87	214	0.79	79
	100	22	183	108	0.89	66.9	0.87	87	214	0.79	79
	200	20	320	84	0.89	53.5	0.93	93	323	0.86	86
4-APD	25	19	140	163	0.85	83.4	0.83	83	147	0.69	69
	50	22	204	113	0.88	67.4	0.89	89	192	0.76	76
	100	22	211	114	0.88	68.8	0.89	89	219	0.80	80
	200	21	219	129	0.86	72.2	0.89	89	220	0.80	80

[33]. Inspection of Table 2 depicts the increase of n values in comparison with 0.1 M HCl solution. The values of n for the three of inhibitors show an increase with increase in inhibitor concentration. This can be attributed to the slightly improvement of surface homogeneity due to inhibitor adsorption on the most active sites. But, variations of n values in the case of 4-ATP is in contrast with other three inhibitors and this phenomenon probably refers to its unique molecular structure.

Considering the EIS results and comparing them with the polarization results at various concentrations of inhibitors, it is clear that

Table 3
Electrochemical parameters obtained from the polarization curves at different temperatures.

T (°C)	Blank		2-ATP			4-ATP			2-APD			4-APD		
	E_{corr} (mV)	i_{corr} (mA/cm^2)	E_{corr} (mV)	i_{corr} (mA/cm^2)	%η	E_{corr} (mV)	i_{corr} (mA/cm^2)	%η	E_{corr} (mV)	i_{corr} (mA/cm^2)	%η	E_{corr} (mV)	i_{corr} (mA/cm^2)	%η
25	−536	1.06	−494	0.14	86	−528	0.19	82	−479	0.07	93	−499	0.13	88
35	−531	1.71	−496	0.22	87	−520	0.24	86	−502	0.23	86	−511	0.37	78
45	−527	1.79	−505	0.36	80	−513	0.34	81	−506	0.35	81	−510	0.41	77
55	−529	2.83	−517	0.77	73	−528	0.67	76	−511	0.58	79	−516	0.58	79

2-ATP and 4-ATP efficiencies are nearly independent of concentration.

3.1.3. Linear polarization resistance (LPR)

LPR method is another useful and fast method for inhibitors study. The effect of inhibitors concentration on LPR value at 25 °C has been measured and listed in Table 2. LPR results confirm the inhibitive properties of present compounds, also conclusions obtained from potentiodynamic polarization and EIS results. In addition, surface coverage and inhibitor efficiency have been calculated by Eq. (4). Although the decrease in efficiencies is not ignorable, these values are close to those calculated by polarization and EIS methods. The difference between obtained efficiencies from LPR and EIS results can be attributed to the fact that, in EIS results, the effect of solution resistance (R_s) is not considered. However the results of LPR method contain this parameter as well as charge transfer resistance. For instance, in EIS results, if the corrosion resistance (R) is considered as the sum of solution resistance (R_s) and charge transfer resistance (R_{ct}), the efficiency value for 200 ppm 2-APD will be 86.43% which is in close correlation with the results obtained from LPR method (86%).

3.2. Effect of temperature

The influence of various temperatures on the specimen corrosion rate has been studied in absence and presence of different inhibitors at 200 ppm in 0.1 M HCl. For this purpose, potentiodynamic polarization has been performed at temperatures differed from 25 to 55 °C in absence and presence of 2-ATP, 4-ATP, 2-APD and 4-APD and extracted electrochemical parameters corresponding to polarization results at various temperatures have been presented in Table 3. It is important to explain the complicated effect of temperature on inhibitor behavior while many changes such as rapid etching, desorption of inhibitor and even inhibitor decomposition on the metal surface may occur [16]. Although, Table 3 data obviously shows an increase in corrosion rate with rising in temperature, however the corrosion rate of inhibited solutions is always lower than the blank one. Considering the corrosion current density (i_{corr}) which corresponds to different temperatures, the activation parameter (E_a) for corrosion process can be obtained using Arrhenius equation:

$$\ln(i_{corr}) = \ln A - \frac{E_a}{RT} \tag{7}$$

By calculating the slope of $\ln(i_{corr})$ vs. $1/T$ plot (Fig. 6), E_a which is an indication of adsorption mechanism, will be obtained. E_a values related to mild steel in 0.1 M HCl solution in absence and presence of the inhibitors has been listed in Table 4. It has been reported that the higher E_a in presence of inhibitors in comparison with blank solution is typically showing physisorption [34]. Considering E_a values, inhibitors tested in this work have an electrostatic interaction on the metal surface (physisorption).

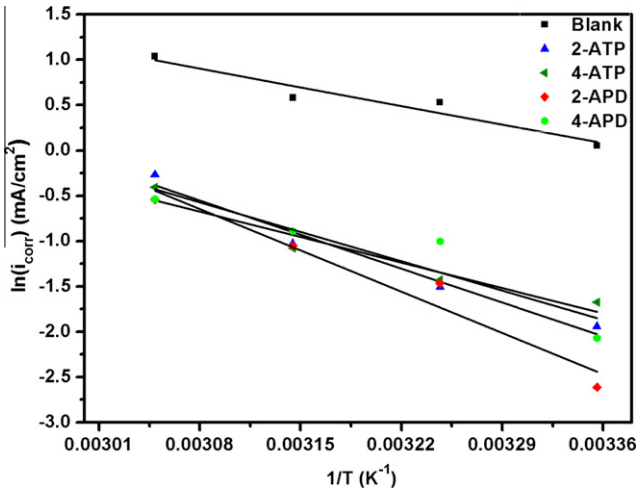

Fig. 6. $\ln(i_{corr})$ vs. $1/T$ for mild steel dissolution in 0.1 M HCl in the absence and presence 200 ppm of inhibitors.

Table 4
Thermodynamic parameters for adsorption of thiophenol derivatives on mild steel surface in 0.1 M HCl solutions.

Inhibitor	E_a (kJ/mol)	ΔG°_{ads} (kJ/mol)	ΔH°_{ads} (kJ/mol)	ΔS°_{ads} (J/mol K)
Blank	24.4	–	–	–
2-ATP	44.5	−35.8	−22.9	43.2
4-ATP	33.5	−38.5	−10.9	92.4
2-APD	54.1	−35.0	−32.6	8.1
4-APD	38.6	−36.8	−16.0	69.7

3.3. Thermodynamic calculations of inhibitor adsorption

Basic thermodynamic information on interaction between inhibitor molecules and metal surface can be provided by adsorption isotherm [16]. There are several adsorption isotherms such as Langmuir, Temkin, Bockris–Swinkels, Flory–Huggins and Frumkin [35]. The type of inhibitor adsorption (chemisorption or physisorption) can be determined using thermodynamic data obtained from isotherms. Adsorption of organic molecules at the metal/solution interface can be elucidated by substitution of them with water molecules on the metal surface [10]:

$$Org_{(sol)} + xH_2O_{(ads)} \rightleftarrows Org_{(ads)} + xH_2O_{(sol)} \tag{8}$$

where $Org_{(sol)}$ and $Org_{(ads)}$ are inhibitor molecules dissolved in solution and adsorbed on metal surface, respectively. Also, $H_2O_{(ads)}$ is adsorbed water molecule on metal surface, $H_2O_{(sol)}$ is water molecule in solution and x is size ratio which represents the number of water molecules replaced with those of inhibitor. Langmuir Isotherm is a suitable model which is generally used for inhibitor studies. According to this model, the surface coverage (θ) is proportional to inhibitor concentration (C) as follows [1,4,11,15,16,18,20–21,36]:

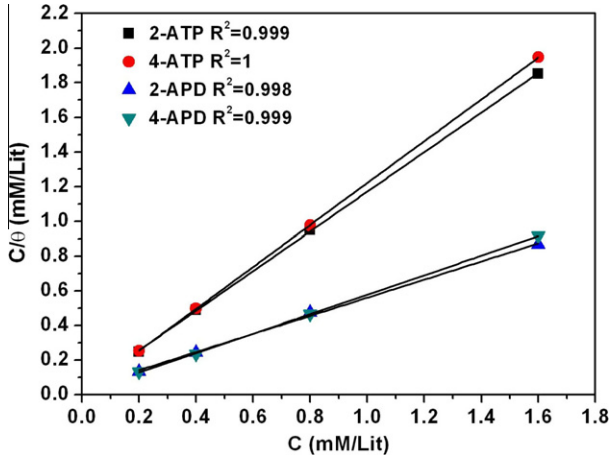

Fig. 7. Langmuir adsorption isotherm of inhibitors in 0.1 M HCl at 25 °C.

$$\frac{\theta}{1-\theta} = K_{ads} \cdot C \tag{9}$$

Then, by rearranging:

$$\frac{C}{\theta} = \frac{1}{K_{ads}} + C \tag{10}$$

In this expression, K_{ads} is equilibrium constant for adsorption reaction. Indeed, values of $R^2 > 0.998$ show that the tested compounds obey Langmuir rule (Fig. 7). According to assumptions of this model, adsorbed molecules occupy only one site and there are no interactions with other adsorbed species [37]. The values of surface coverage (θ), calculated by using Tafel polarization data, corresponds to different concentrations of the inhibitor, have been applied to determine the adsorption isotherm. Meanwhile, K_{ads} can be calculated from the intercept line on C/θ axis and further, ΔG°_{ads} can be obtained from K_{ads} by the use of following equation [4–5,16,23,38]:

$$\Delta G^{\circ}_{ads} = -RT \ln(55.5 K_{ads}) \tag{11}$$

In this expression, R is gas constant, T is absolute temperature and 55.5 is concentration of water in solution in mol/l. ΔG°_{ads} values corresponding to present inhibitors have been calculated and presented in Table 4. The negative sign of ΔG°_{ads} refers to the adsorption of inhibitors onto the metal surface [37,39]. In general, the magnitude of ΔG°_{ads} approximately −20 kJ/mol or less negative is assumed for existing electrostatic interactions between inhibitor and the charged metal surface (i.e., physisorption). Those ΔG°_{ads} around −40 kJ/mol or more negative are an indication of charge sharing or charge transferring from an organic specie to the metal surface to form a coordinate type of metallic bond (i.e., chemisorption) [16]. Despite the nearly similar ΔG°_{ads} values for all inhibitors, 4-ATP can be considered as most stable compound from adsorption stand point, having the highest ΔG°_{ads} value.

Gibbs–Helmholtz equation can be used to calculate the heat of adsorption process (ΔH°_{ads}). With good estimation, Δc_p reaction can be considered as constant value, thus ΔH° of reaction and Gibbs–Helmholtz equation will appear as follows:

$$\Delta H^{\circ} = \Delta c_p T + A \tag{12}$$

$$\ln(K) = \frac{\Delta c_p}{R} \ln T - \frac{A}{RT} + B \tag{13}$$

where A and B are equation constants and K is equilibrium constant of reaction. Using Eqs. (9), (11), and (13), the surface coverage is related to temperature:

$$\ln\left(\frac{\theta}{1-\theta}\right) = \frac{\Delta c_p}{R} \ln T - \frac{A}{RT} + B' \tag{14}$$

In which, θ and B' are surface coverage and equation constant, respectively. By solving Eq. (14) for different surface coverage in presence of 200 ppm inhibitor at various temperatures (Table 3), Δc_p and A constants were obtained and according to Eq. (12), ΔH°_{ads} was calculated at 298 K and presented in Table 4.

The entropy of adsorption process (ΔS°_{ads}) can also be calculated based on the following thermodynamic equation [16,37]:

$$\Delta G^{0}_{ads} = \Delta H^{0}_{ads} - T\Delta S^{0}_{ads} \tag{15}$$

Invaluable information about the mechanism of corrosion inhibition can be provided by the calculated values of thermodynamic parameters for the adsorption of inhibitors; see Table 4. An endothermic adsorption process ($\Delta H^{\circ}_{ads} > 0$) is due to chemisorption while an exothermic one ($\Delta H^{\circ}_{ads} < 0$) may be attributed to physisorption, chemisorption or a mixture of both [16]. For physisorption processes, this magnitude is usually lower than 40 kJ/mol while it usually is close to 100 kJ/mol in chemisorptions [34]. In this work, the values of ΔH°_{ads} are indicating physisorption mechanism that is in agreement with results obtained by activation parameter (E_a).

The positive signs of ΔS°_{ads} for all inhibitors are related to the substitutional process, which can be attributed to the increase in water desorption entropy [29,40]. It could be interpreted that inhibitor molecules can desorb water molecules from the metal surface, causing an increase in disorders of system [16,37]. The values of ΔS°_{ads} for present compound show that the inhibitor with lowest ΔS°_{ads} value has higher efficiency. In other word, it can be claimed the molecule which adsorbs at surface with better order produces higher protection against corrosion. This behavior is also seen in inhibitors investigated by some researchers (see Ref. [10]).

3.4. Corrosion attack morphology

Corrosion attack morphologies in absence and presence of different inhibitors have been investigated by employing optical microscopy and presented in Fig. 8. In absence of the inhibitor (Fig. 8a), the specimen surface has been severely corroded. At same time, the corrosion attack is significantly lower than uninhibited

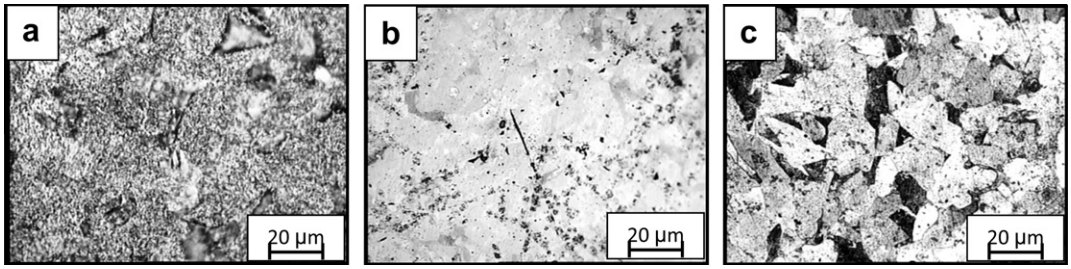

Fig. 8. Corrosion attack morphology (a) blank solution after 1.5 h, (b) in presence of 200 ppm of 2-APD after 1.5 h and (c) in presence of 200 ppm of 2-ATP after 1.5 h.

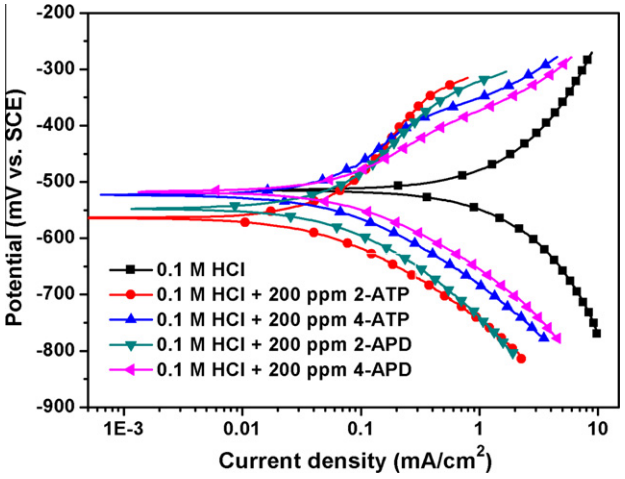

Fig. 9. Effect of time on the potentiodynamic behavior of mild steel in blank and 200 ppm inhibited solutions at 25 °C.

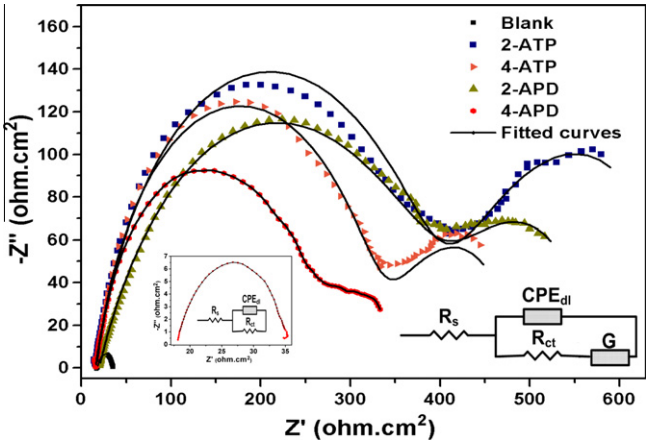

Fig. 10. Effect of time on Nyquist plot of inhibited and uninhibited solutions at 25 °C.

solution in presence of inhibitors. For instance, the surface of specimen in presence of 200 ppm 2-APD in 0.1 M HCl, has not been corroded. Surface evaluation of specimen immersed during 1.5 h, reveals that mirror-like polished specimen surface has been just partially etched after immersion test, while the surface of specimen in absence of inhibitor has changed to rough and a black appearance due to severe corrosion. In addition, in the case of 2-ATP (results of 4-ATP and 4-APD are similar to 2-ATP) which has lower efficiency than 2-APD, grain boundaries and pearlite phase are more visible, indicating higher corrosion attack.

3.5. Effect of immersion time

3.5.1. Potentiodynamic polarization

To investigate the effect of immersion time on inhibitor behavior, potentiodynamic polarization tests have been carried out in absence and presence of 200 ppm concentration of inhibitors after 24 h immersion at 25 °C (Fig. 9). Electrochemical parameters related to these curves have been extracted and presented in Table 5. A comparison between the result of uninhibited solution after 1 and 24 h of immersion obviously shows an increase in corrosion current density with time passage. The reason for this observation can be related to an increase in metal surface because of the excess dissolution of iron [29]. It is noticeable that exposure of specimen after 24 h in blank solution tends to more deterioration of mild steel surface. In presence of inhibitors, the decrease in current density of mild steel specimen is a positive phenomenon. This decrease in corrosion rate is considerably seen in the case of 2-ATP and 4-ATP. One reason for the increase in corrosion resistance can be associated to more substitution of inhibitor molecules with water ones at surface. Table 5 data reveals that E_{corr} changes toward more positive values after 24 h immersion in the blank solution. The increase in Fe^{2+} activity and consequently the reversible electrochemical potential of anodic reaction may increase corrosion potential.

3.5.2. Electrochemical impedance spectroscopy

Nyquist plots and their fitted curves after 24 h immersion in absence and presence of 200 ppm of all inhibitors have been presented in Fig. 10. Long term EIS plots show an interesting behavior in comparison with short time ones. Their short time apparent feature changes and a new element becomes visible namely Gerischer at equivalent circuit. A suitable concurrency between experimental and simulated Nyquist plots can be a confirmation on existence of Gerischer Impedance. In 1951, Gerischer published the formal treatment of the DC and AC response for a CE-type reaction (a chemical reaction followed by an electrochemical one) at an inert electrode on an aqueous electrolyte [41]. In 1984, Sluyters-Rehbach published the complete impedance expression for a CEC type reaction (chemical–electrochemical–chemical, i.e., an electrochemical reaction preceded and followed by a chemical reaction) which was suitably named the Gerischer Impedance [41]. The Gerischer element appears in most of the equivalent circuit fitting programs, but many people are unsure of its meaning. This element is more complicated than Warburg impedance, (Z_W), which has an additional parameter (K) as a transfer rate (s^{-1}) for chemical reactions [41,42]. According to the following equation, if $K = 0$, this element has no difference with Warburg element:

$$Z_G(\omega) = \frac{Y}{\sqrt{k + i\omega}} \tag{16}$$

The Y parameter has the same definition as the Warburg impedance and can be used to calculate the diffusion coefficient for the mobile species using same equations as for the Warburg.By investigating

Table 5
Electrochemical parameters extracted from the polarization curves and EIS indices obtained from the Nyquist plots after 24 h at 25 °C.

Inhibitor	Polarization			EIS							
	E_{corr} (mV)	i_{corr} (mA/cm^2)	%η	R_s (Ω cm^2)	R_{ct} (Ω cm^2)	CPE$_{dl}$		C_{dl} (μF/cm^2)	G		%η
						P (μF/cm^2)	n		Y_o (Ω S$^{1/2}$)	K (S^{-1})	
Blank	−514	1.216	–	18	17	4555	0.80	2403	–	–	–
2-ATP	−565	0.048	96	16	374	111	0.80	50.3	0.016	0.056	95
4-ATP	−524	0.049	96	17	311	140	0.84	77.1	0.025	0.071	95
2-APD	−547	0.055	96	20	380	262	0.68	88.1	0.024	0.067	96
4-APD	−517	0.070	94	15	251	299	0.80	156	0.035	0.097	93

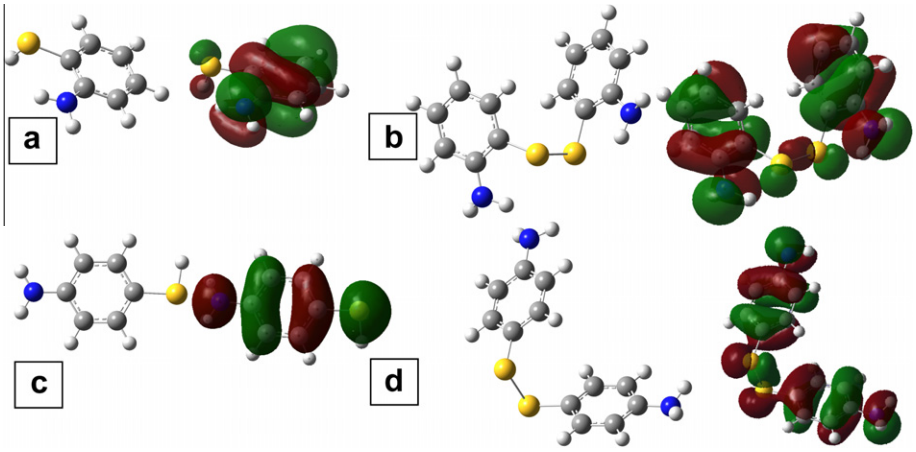

Fig. 11. Optimized molecular structure and HOMO of (a) 2-ATP, (b) 4-ATP, (c) 2-APD and (d) 4-APD.

the extracted data from equivalent circuits presented in Table 5 an increase in charge transfer resistance after 24 h immersion is observable. This phenomenon can be attributed to substitution of more inhibitor molecules with water ones and as a result, a decrease in active dissolution and hydrogen evolution sites. In addition, existence of Gerischer impedance in equivalent circuit could be further discussed by some reasons. Probably, one could be formation of cross-linked connections between inhibitor molecules by Fe^{2+}. Lone electrons pairs of sulfur atoms and vacant orbitals of Fe^{2+} can cause to form a dative bond between every two inhibitor molecules and consequently lead to coupling inhibitors together. Similar mechanism has been previously reported for inhibitor studies on copper in NaCl solution [43]. Another reason might be addressed to synthesizing of different organic compounds by the existence of Fe ions which act as catalyst in the system [24]. Overall, both EIS and polarization result confirms improvement of inhibitive behavior of all present inhibitors especially in the case of 2-ATP by passing time.

3.6. Quantum chemical study

Quantum chemical study has been carried out for investigating the relationship between the molecular structure of present inhibitors and their inhibition effect. Geometric structures and electronic properties of 2-ATP, 4-ATP, 2-APD and 4-APD have been calculated by DFT method using B3LYP level and 3–21G** basis set. Fig. 11 is illustrating optimized molecular structures and high occupied molecular orbital (HOMO) and demonstrating that the benzene ring, S and N atoms have larger electric density. Type of benzene ring electrons is π-bonding electrons while for S and N atoms those are non-bonding electrons pair. It is suggested that the benzene ring, S and N atoms can be suitable places for adsorption onto surface, especially in the case of S and N atoms because of having lone pairs of electrons. Molecules of present inhibitors can be directly adsorbed at the steel surface on the basis of donor–acceptor interactions between π-electrons of benzene ring, non-bonding lone pairs of S and N atoms, and vacant *d*-orbitals of iron atoms. Therefore, the deference in tested inhibitors efficiencies refers to their various molecular structures.

Quantum chemical indices containing E_{HOMO} and E_{LUMO} have been presented in Table 6. The main difference between these molecules concerns the E_{LUMO} values. E_{LUMO} values are significantly different for synthesized and non-synthesized molecules. Organic compounds with lower E_{LUMO}, greater adsorption ability and better corrosion inhibition properties are expected. It has been reported that excellent inhibition corrosion properties are usually obtained using organic compounds that not only offer electrons to unoccupied orbitals of the metal but also accept free electrons from the metal by using their anti-bond orbitals to form stable chelates [3]. Indeed, this behavior is observed in present inhibitors and compounds with lower E_{LUMO} values give higher inhibition efficiencies.

Table 6
HOMO and LUMO values of studied thiophenol derivatives calculated by DFT method.

	2-ATP	4-ATP	2-APD	4-APD
E_{HOMO} (eV)	−5.74	−5.11	−5.66	−5.57
E_{LUMO} (eV)	−0.571	−0.244	−1.82	−1.39

4. Conclusions

In this study, inhibitive performance of some thiophenol derivatives on corrosion behavior of mild steel in 0.1 M HCl solution has been investigated and following main results obtained:

1. All compounds have good inhibitive effect with noticeable efficiencies and could be listed in order of 2-APD > 4-APD > 2-ATP > 4-ATP if they are compared at 200 ppm concentration.
2. Investigating effect of inhibitors concentration on their efficiency shows that 2-ATP and 4-ATP have corrosion current densities nearly independent of their concentrations while in the case of 2-APD and 4-APD, it increases with increasing their concentration especially in net anodic current densities.
3. Evaluating temperature effect on efficiency of investigated compounds at 200 ppm concentration shows despite the corrosion current densities increases with rising temperature, they always are lower than blank solution one.
4. Exploring the effect of time on inhibitors behavior by EIS technique reveals the decrease in corrosion rate and declares a new concept in study of inhibitors with appearance of Gerischer element in equivalent circuit.
5. Adsorption of present inhibitors obeys Langmuir rule and thermodynamic data extracted by this rule is showing physical adsorption.
6. Optical microscopy obviously shows the corrosion attack morphology in absence and presence of inhibitors in 0.1 M HCl solution and it depicts that mild steel surface severely corrodes if inhibitors are not used.
7. Quantum chemical study reveals that the benzene ring, S and N atoms can be suitable sites for adsorption onto surface. This is pronounced for S and N because of having lone pair of electrons.

Acknowledgments

The authors appreciate the financial support from Ferdowsi University of Mashhad provision of laboratory facilities during the period that this research was conducted and Dr. H.A. Moradi and Dr. G.h. Farhadipour for their invaluable helps.

References

[1] M. Behpour, S.M. Ghoreishi, N. Mohammadi, N. Soltani, M. Salavati-Niasari, Investigation of some Schiff base compounds containing disulfide bond as HCl corrosion inhibitors for mild steel, Corros. Sci. 52 (2010) 4046–4057.
[2] R. Goel, W.A. Siddiqi, B. Ahmed, M.S. Khan, V.M. Chaubey, Synthesis characterization and corrosion inhibition efficiency of N-C2 (2E)-2-[4-(dimethylamino) benzylidene] hydrazinyl 2-oxo ethyl benzamide on mild steel, Desalination 263 (2010) 45–57.
[3] L. Herrag, B. Hammouti, S. Elkadiri, A. Aouniti, C. Jama, H. Vezin, F. Bentiss, Adsorption properties and inhibition of mild steel corrosion in hydrochloric solution by some newly synthesized diamine derivatives: experimental and theoretical investigations, Corros. Sci. 52 (2010) 3042–3051.
[4] N.A. Negm, Y.M. Elkholy, M.K. Zahran, S.M. Tawfik, Corrosion inhibition efficiency and surface activity of benzothiazol-3-ium cationic Schiff base derivatives in hydrochloric acid, Corros. Sci. 52 (2010) 3523–3536.
[5] R. Solmaz, Investigation of the inhibition effect of 5-((*E*)-4-phenylbuta-1, 3-dienylideneamino)-1,3,4-thiadiazole-2-thiol Schiff base on mild steel corrosion in hydrochloric acid, Corros. Sci. 52 (2010) 3321–3330.
[6] D.K. Yadav, B. Maiti, M.A. Quraishi, Electrochemical and quantum chemical studies of 3,4-dihydropyrimidin-2(1*H*)-ones as corrosion inhibitors for mild steel in hydrochloric acid solution, Corros. Sci. 52 (2010) 3586–3598.
[7] B. Sanyal, Organic compounds as corrosion inhibitors in different environments – a review, Prog. Org. Coat. 9 (1981) 165–236.
[8] I. Ahamad, R. Prasad, M.A. Quraishi, Experimental and quantum chemical characterization of the adsorption of some Schiff base compounds of phthaloyl thiocarbohydrazide on the mild steel in acid solutions, Mater. Chem. Phys. 124 (2010) 1155–1165.
[9] I. Ahamad, R. Prasad, M.A. Quraishi, Inhibition of mild steel corrosion in acid solution by Pheniramine drug: experimental and theoretical study, Corros. Sci. 52 (2010) 3033–3041.
[10] J. Aljourani, K. Raeissi, M.A. Golozar, Benzimidazole and its derivatives as corrosion inhibitors for mild steel in 1 M HCl solution, Corros. Sci. 51 (2009) 1836–1843.
[11] S. Deng, X. Li, H. Fu, Nitrotetrazolium blue chloride as a novel corrosion inhibitor of steel in sulfuric acid solution, Corros. Sci. 52 (2010) 3840–3846.
[12] H. Ju, Z.-P. Kai, Y. Li, Aminic nitrogen-bearing polydentate Schiff base compounds as corrosion inhibitors for iron in acidic media: a quantum chemical calculation, Corros. Sci. 50 (2008) 865–871.
[13] S. Zhang, Z. Tao, W. Li, B. Hou, The effect of some triazole derivatives as inhibitors for the corrosion of mild steel in 1 M hydrochloric acid, Appl. Surf. Sci. 255 (2009) 6757–6763.
[14] P. Zhao, Q. Liang, Y. Li, Electrochemical, SEM/EDS and quantum chemical study of phthalocyanines as corrosion inhibitors for mild steel in 1 mol/l HCl, Appl. Surf. Sci. 252 (2005) 1596–1607.
[15] F. Bentiss, M. Lagrenee, M. Traisnel, J.C. Hornez, The corrosion inhibition of mild steel in acidic media by a new triazole derivative, Corros. Sci. 41 (1999) 789–803.
[16] F. Bentiss, M. Lebrini, M. Lagrenée, Thermodynamic characterization of metal dissolution and inhibitor adsorption processes in mild steel/2,5-bis(*n*-thienyl)-1,3,4-thiadiazoles/hydrochloric acid system, Corros. Sci. 47 (2005) 2915–2931.
[17] F. Bentiss, M. Traisnel, L. Gengembre, M. Lagrenée, A new triazole derivative as inhibitor of the acid corrosion of mild steel: electrochemical studies, weight loss determination, SEM and XPS, Appl. Surf. Sci. 152 (1999) 237–249.
[18] M. El Azhar, B. Mernari, M. Traisnel, F. Bentiss, M. Lagrenée, Corrosion inhibition of mild steel by the new class of inhibitors [2,5-bis(*n*-pyridyl)-1,3,4-thiadiazoles] in acidic media, Corros. Sci. 43 (2001) 2229–2238.
[19] M. Lebrini, M. Traisnel, M. Lagrenée, B. Mernari, F. Bentiss, Inhibitive properties, adsorption and a theoretical study of 3,5-bis(*n*-pyridyl)-4-amino-1,2,4-triazoles as corrosion inhibitors for mild steel in perchloric acid, Corros. Sci. 50 (2008) 473–479.
[20] F. Bentiss, B. Mernari, M. Traisnel, H. Vezin, M. Lagrenée, On the relationship between corrosion inhibiting effect and molecular structure of 2,5-bis(*n*-pyridyl)-1,3,4-thiadiazole derivatives in acidic media: ac impedance and DFT studies, Corros. Sci. 53 (2010) 487–495.
[21] K.F. Khaled, Corrosion control of copper in nitric acid solutions using some amino acids – a combined experimental and theoretical study, Corros. Sci. 52 (2010) 3225–3234.
[22] K.F. Khaled, Electrochemical investigation and modeling of corrosion inhibition of aluminum in molar nitric acid using some sulphur-containing amines, Corros. Sci. 52 (2010) 2905–2916.
[23] M.K. Pavithra, T.V. Venkatesha, K. Vathsala, K.O. Nayana, Synergistic effect of halide ions on improving corrosion inhibition behaviour of benzisothiozole-3-piperizine hydrochloride on mild steel in 0.5 M H_2SO_4 medium, Corros. Sci. 52 (2010) 3811–3819.
[24] H. Eshghi, M. Bakavoli, H. Moradi, A. Davoodnia, $Fe(HSO_4)_3$ and $Fe(HSO_4)_3$/DMSO as efficient, heterogeneous, and reusable catalyst systems for the oxidative coupling of thiols, Phosphorus Sulfur Silicon Relat. Elem. 184 (2009) 3110–3118.
[25] E. McCafferty, Validation of corrosion rates measured by the Tafel extrapolation method, Corros. Sci. 47 (2005) 3202–3215.
[26] G.E. Badr, The role of some thiosemicarbazide derivatives as corrosion inhibitors for C-steel in acidic media, Corros. Sci. 51 (2009) 2529–2536.
[27] E. McCafferty, N. Hackerman, Double layer capacitance of iron and corrosion inhibition with polymethylene diamines, J. Electrochem. Soc. 119 (1972) 146–154.
[28] A.A. Aksüt, W.J. Lorenz, F. Mansfeld, The determination of corrosion rates by electrochemical d.c. and a.c. methods. II: Systems with discontinuous steady state polarization behavior, Corros. Sci. 22 (1982) 611–619.
[29] R. Solmaz, G. Kardas, M. Çulha, B. YazIcI, M. Erbil, Investigation of adsorption and inhibitive effect of 2-mercaptothiazoline on corrosion of mild steel in hydrochloric acid media, Electrochim. Acta 53 (2008) 5941–5952.
[30] B. Hirschorn, M.E. Orazem, B. Tribollet, V. Vivier, I. Frateur, M. Musiani, Determination of effective capacitance and film thickness from constant-phase-element parameters, Electrochim. Acta 55 (2010) 6218–6227.
[31] H.H. Hassan, Perchlorate and oxygen reduction during Zn corrosion in a neutral medium, Electrochim. Acta 51 (2006) 5966–5972.
[32] A.K. Singh, M.A. Quraishi, Effect of Cefazolin on the corrosion of mild steel in HCl solution, Corros. Sci. 52 (2010) 152–160.
[33] F. Bentiss, M. Traisnel, M. Lagrenee, The substituted 1,3,4-oxadiazoles: a new class of corrosion inhibitors of mild steel in acidic media, Corros. Sci. 42 (2000) 127–146.
[34] E.A. Noor, A.H. Al-Moubaraki, Thermodynamic study of metal corrosion and inhibitor adsorption processes in mild steel/1-methyl-4[4′(-X)-styryl pyridinium iodides/hydrochloric acid systems, Mater. Chem. Phys. 110 (2008) 145–154.
[35] A. Ghanbari, M.M. Attar, M. Mahdavian, Corrosion inhibition performance of three imidazole derivatives on mild steel in 1 M phosphoric acid, Mater. Chem. Phys. 124 (2010) 1205–1209.
[36] T. Arslan, F. Kandemirli, E.E. Ebenso, I. Love, H. Alemu, Quantum chemical studies on the corrosion inhibition of some sulphonamides on mild steel in acidic medium, Corros. Sci. 51 (2009) 35–47.
[37] G. Avci, Corrosion inhibition of indole-3-acetic acid on mild steel in 0.5 M HCl, Colloid Surf. A 317 (2008) 730–736.
[38] R. Sayós, M. González, J. Costa, On the use of quantum chemical methods as an additional tool in studying corrosion inhibitor substances, Corros. Sci. 26 (1986) 927–934.
[39] H. Amar, A. Tounsi, A. Makayssi, A. Derja, J. Benzakour, A. Outzourhit, Corrosion inhibition of Armco iron by 2-mercaptobenzimidazole in sodium chloride 3% media, Corros. Sci. 49 (2007) 2936–2945.
[40] X. Li, S. Deng, H. Fu, G. Mu, Inhibition effect of 6-benzylaminopurine on the corrosion of cold rolled steel in H_2SO_4 solution, Corros. Sci. 51 (2009) 620–634.
[41] B.A. Boukamp, H.J.M. Bouwmeester, Interpretation of the Gerischer impedance in solid state ionics, Solid State Ionics 157 (2003) 29–33.
[42] B.A. Boukamp, M. Verbraeken, D.H.A. Blank, P. Holtappels, SOFC-anodes, proof for a finite-length type Gerischer impedance, Solid State Ionics 177 (2006) 2539–2541.
[43] M. Finsgar, I. Milosev, Inhibition of copper corrosion by 1,2,3-benzotriazole: a review, Corros. Sci. 52 (2010) 2737–2749.